Chemical Physics Letters 538 (2012) 102–107

Contents lists available at SciVerse ScienceDirect

Chemical Physics Letters

journal homepage: www.elsevier.com/locate/cplett

Photoelectrochemical responses of silicon nanowire arrays for light detection

Shao-long Wu, Ting Zhang, Rui-ting Zheng, Guo-an Cheng *

Key Laboratory of Beam Technology and Material Modification of Ministry of Education, College of Nuclear Science and Technology, Beijing Normal University, Beijing 100875, PR China

ARTICLE INFO

Article history:
Received 16 November 2011
In final form 21 April 2012
Available online 27 April 2012

ABSTRACT

This Letter presents a novel low-cost light detector based on radial silicon nanowire heterostructures. Photoelectrochemical responses of silicon nanowire arrays with different morphologies, prepared by a metal assisted chemical etching method, have been systematically investigated. The photoresponsivity of the black silicon nanowire arrays is 73 times larger than that of the planar silicon at 0.2 V bias under white light illumination. The relationship between the photoresponsivity and nanowire morphology and doping level is discussed. Our results demonstrate that the heterostructures of the nanowire arrays with an optimized morphology are promising for light detection and other optoelectronic devices.

1. Introduction

In the last two decades, one dimensional semiconductor nanostructure (1DSNS) arrays have attracted much attention due to their unique physical and chemical properties, such as novel thermoelectricity, high selective adsorption of gas, and enhanced biological and chemical sensitivity [1–3]. Besides, photoconductivity is another hot issue for the 1DSNS, which exhibits promising applications in photovoltaics, photodetectors, optical switches, optical interconnects and transceivers [4–7]. Photoconductivity involves several successive or simultaneous processes, namely light absorption, carrier photogeneration, carrier transmitting (including carrier trapping, detrapping and recombination), and carrier collection. Since 1DSNS arrays show excellent optical absorption due to the combined effects of light funneling, light scattering and light polarization [8–10], the photodetectors of 1DSNS arrays are promising.

Conventional concepts and architectures of optoelectronic devices, such as p-n junction, metal–semiconductor junction and phototransistors, have been replicated on the 1DSNS photodetectors by means of axial homostructures or heterostructures with electrical contacts at the two terminals of individual 1DSNS [11] or 1DSNS arrays [12]. However, the collection efficiency of photogenerated carriers is relatively low in these structures due to the limited junction area, short minority-carrier diffusion length, and long overall transmitting distances of effective carriers. Moreover, compared with bulk materials, the recombination barrier height in 1DSNS may be reduced due to the pinning effect of Fermi level [13,14], resulting in an increase of the recombination of photogenerated carriers. To balance the requirements for light absorption and photogenerated carrier collection, 1DSNS arrays with radial p-n (or other) junctions are proposed. The directions of light absorption and carrier transport in these structures are perpendicular. Each individual 1DSNS could be long in the direction of incident light, allowing for optimal light absorption, but thin in another dimension, thereby allowing for effective carrier collection.

Lauhon et al. [15] synthesized Si and Ge core–shell nanowire (NW) heterostructures using a chemical vapor deposition (CVD)-based epitaxial shell-growth method. Their experiments demonstrated that the radial heterostructures would significantly improve the performances of the existing NW-based devices. Jeong et al. [16] fabricated the three-dimensional (3D) ZnO NW hybrid structure by growing a ZnO buffer layer, ZnO NW arrays, and a ZnO film in sequence by a metal–organic CVD method, and observed that the photocurrent of the hybrid structure was generated only under ultraviolet (UV) light illumination, suggesting its application potentials in the UV detectors. However, there are still great challenges in controlling the uniformity of junctions, simplifying the fabrication processes and reducing the cost. Herein, we propose a novel light detector based on the radial heterostructures of the 1DSNS arrays. The heterostructures were fabricated by a relatively simple and cheap method. The device photosensitivities based on the SiNW arrays with two different morphologies were systematically investigated, with comparison to that of the planar Si heterostructures. Our results demonstrate that the radial heterostructures of 1DSNS arrays have promising potentials for light detection.

2. Experimental details

The SiNW arrays were prepared by the metal assisted chemical etching of n-type Si(100) wafers with a resistivity of 2–2.7 Ω cm [7,17]. Two kinds of SiNW arrays with different morphologies (i.e. black arrays and gray arrays, named according to their color

* Corresponding author. Fax: +86 010 62205403.
E-mail address: gacheng@bnu.edu.cn (G.-a. Cheng).

0009-2614/$ - see front matter © 2012 Elsevier B.V. All rights reserved.
http://dx.doi.org/10.1016/j.cplett.2012.04.046

appearances) were obtained by adjusting etching conditions. The cut Si chips with an area of ~2 × 2 cm^2 were cleaned ultrasonically in deionized water, acetone and ethanol for 10 min in sequence, and then boiled in the H_2SO_4/H_2O_2 (4/1 by volume) for 15 min. The cleaned Si chips were kept in deionized water for use. For the preparation of SiNW arrays, the cleaned Si chips were dipped into the HF dilute solution for 2 min to remove silicon oxide layer, and then immersed into the aqueous solution mixed with 4 M HF and 0.01 M $AgNO_3$ for 1 min to deposit Ag nanoparticles (AgNPs). After that, the AgNP-coated Si chips were soaked into the aqueous solution mixed with 4 M HF and 0.2 M H_2O_2 for 10 min at room temperature (~20 °C). Finally, the black SiNW arrays were obtained. The gray SiNW arrays were prepared via secondary metal assisted chemical etching, in which the as-etched black SiNW arrays were dipped into the aqueous solution mixed with 4 M HF and 0.005 M $AgNO_3$ for 10 s, and then soaked into the aqueous solution mixed with 4 M HF and 0.4 M H_20_2 for 10 min. Both of the black and gray arrays were cleaned in the boiled 50 vol.% HNO_3 for 1 h to remove the residual AgNPs, following washed by deionized water and then dried for use.

The morphologies and structures of the SiNW arrays were characterized by a field emission scanning electron microscope (*FE-SEM, Hitachi S-4800*) and a high resolution transmission electron microscope (*HR-TEM, JEOL JEM-2010*). Reflectance and transmission spectra were obtained by a UV–Vis spectrophotometer equipped with an integrating sphere (*SPECORD 200, Analytik Jena AG*).

The photoelectrochemical responses were measured in a two-electrode configuration, as shown in Figure 2a, which was composed of an electrochemical workstation (*CS300, WUHAN CORRTEST INSTRUMENT CO. LTD*), an electrolytic cell and a white light illumination system (*SHENZHEN LTWG ELECTRONICS CO. Ltd.*). The SiNW arrays and planar Si were used as the photoelectode, and the Pt mesh was used as the counter electrode and reference electrode. All the voltage values in this Letter correspond to the Pt electrode. The electrolyte solution was a mixed solution of 40 wt.% hydrogen bromide and 3 wt.% bromine liquid with a volume ratio of 4/1. The wavelengths of light illumination was in the range of 420–760 nm, and the total illumination intensity was ~1560 μW/cm^2, determined by a visible light irradiatometer (*FZ-A, Photoelectric Instrument Factory of Beijing Normal University*). The photoelectrodes were prepared by sputtering an aluminum layer with ~1 μm thickness on the backs of the arrays and planar Si chips, and post-annealing at 450 °C for 55 s in a rapid thermal processing system within N_2 atmosphere. The electrochemical workstation was used to supply applied voltages and record currents. A pulse light illumination obtained by a pulse power source was used to determine the ON–OFF illumination cycles.

3. Results and discussion

To investigate the influence of the morphology of the 1DSNS arrays on their photosensitivity, we prepared two kinds of SiNW arrays with different morphologies. Figure 1 is typical morphological and structural images of the black SiNW arrays and gray SiNW arrays, which shows that the NWs in the black arrays are distinguishable and smooth. However, the NWs in the gray arrays are relatively sparse and rough, and the overall thickness of native oxide layer is larger than that of the NWs in the black arrays. Moreover, the NWs/substrate interface of the gray arrays is uneven. The differences arise from different fabricating processes. The gray SiNW arrays were prepared via secondary metal assisted chemical etching. During the secondary electroless deposition, some AgNPs were precipitated on the tops and side surfaces of the as-etched nanostructures, which could result in the secondary etching. As a result, the NWs in the gray arrays are sparser and rougher than that in the black arrays (as shown in Figure 1a–c and e–g. The thicker oxide layer of the NWs from gray arrays can be attributed to their rougher surface topography and higher surface energy (as shown in Figure 1d and h).

Figure 2a is the schematics of the photoelectrochemical response measurements. The SiNW arrays served as the photoelectrodes in Br/Br^- redox electrolyte. When the as-prepared SiNW arrays were immersed into the electrolyte, 3D 'bulk' heterostructures were formed at the SiNWs/electrolyte interface, as shown in Figure 2b. The light was illuminated along the axial direction of the NWs, and the photogenerated carriers were separated and collected in the radial direction of the NWs. The Fermi level of n-type Si equilibrates with the electrochemical potential of the redox pair, leading to upward bending of band edges [14]. The region of the bending band is referred to as depletion region, and the band bending indicates differences of carrier density in different regions of the electrodes. For an n-type semiconductor NW, the electron density is the highest in the center and the lowest at the surface [6]. Additionally, a positive applied voltage can intensify the bending, thereby facilitating the extraction of photogenerated carriers [14]. Under light illumination with sufficient energy at a positive bias, millions of electron–hole pairs are generated and separated, namely a great number of electrons are promoted to conduction band and then transferred into the Si interior, while the holes are transferred into the solution to oxidize Br^-, resulting in a measurable photocurrent, as shown in Figure 2c. However, the current in the dark at a positive bias is very limited due to few movable electrons at the interface and low-density hole in the n-type Si. The obvious current variations in the dark and under light illumination suggest the photosensitivity of the devices.

Figure 3 shows the photoelectrochemical responses of the SiNW arrays and planar Si with ON–OFF illumination cycles at 0.2 and 1.0 V bias, respectively. In the dark, the currents of all the photoelectrodes are very low. However, there are observable photocurrents when there is light illumination. At 0.2 V bias, the photocurrent density (J_{ph}) of the black arrays is ~910 μA/cm^2, and that of the gray arrays is ~208 μA/cm^2, both of the two J_{ph} are much higher than that of the planar Si (~12.5 μA/cm^2). Meanwhile, the dark current densities (J_{dark}) of the arrays are a little higher than that of the planar Si. The photoresponsivity (R) of devices is calculated by the following equation:

$$R = \frac{J_{PC}}{P_{opt}} = \frac{J_{ph} - J_{dark}}{P_{opt}} \quad (1)$$

where J_{PC} is the photogenerated current density, J_{ph} is the photocurrent density, P_{opt} is the illumination power density. In our experiments, the R of the black arrays is 0.582 A/W, 73 times larger than that of the planar Si (0.008 A/W). When the bias is changed to be 1.0 V, the J_{ph} of the planar Si increases up to ~664 μA/cm^2, while that of the arrays are almost constant. The J_{ph}, J_{dark}, J_{PC}, and R of the black arrays, gray arrays and planar Si at 0.2 and 1.0 V bias are summarized in Table 1.

To further understand the photoelectrochemical responses of the Si-based photoelectrodes with different morphologies, we measured current density (J) as a function of applied voltage (V) using an increasing voltage from −1.5 to 1.5 V with an increasing rate of 25 mV/s both under light illumination and in the dark. From Figure 4, it can be observed that all the three photoelectrodes exhibit a nearly rectifying effect in the dark. Only when the applied voltages are smaller than a certain negative value, are there observable currents. And in the case, the J–V curves with or without light illumination are almost overlapped. However, when the voltages are larger than the certain negative value, the currents under light illumination increase with increasing applied voltages and then reach saturation. These characteristics of these photoelectrodes are consistent with Lauhon's report [15], which can be explained

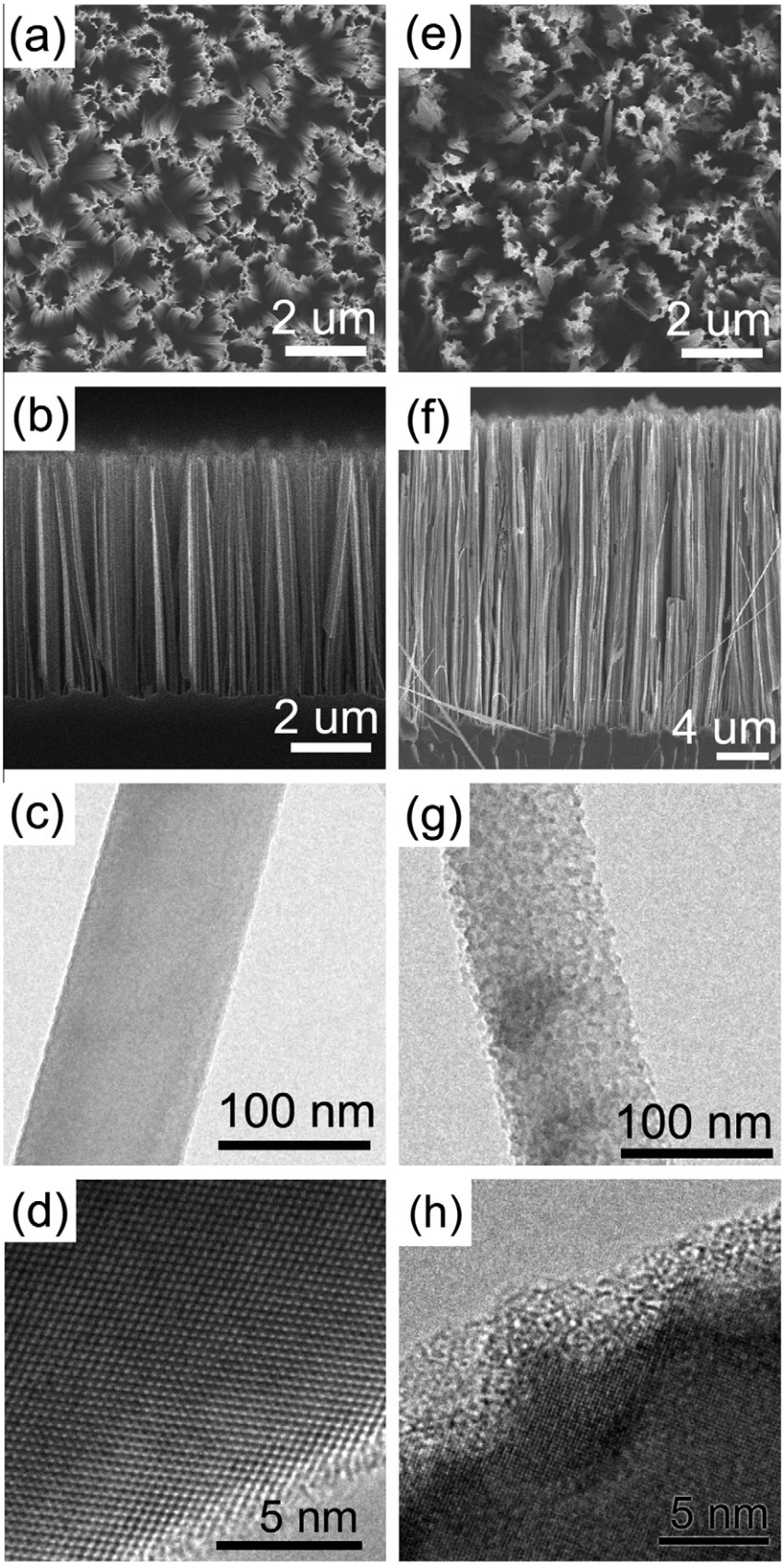

Figure 1. Typical morphologies of the black SiNW arrays and gray SiNW arrays. Top view (a) and cross-sectional (b) view of the black arrays. TEM (c) and HR-TEM (d) images of the NW from the black arrays. Top view (e) and cross-sectional (f) view of the gray arrays. TEM (g) and HR-TEM (h) images of the NW from the gray arrays.

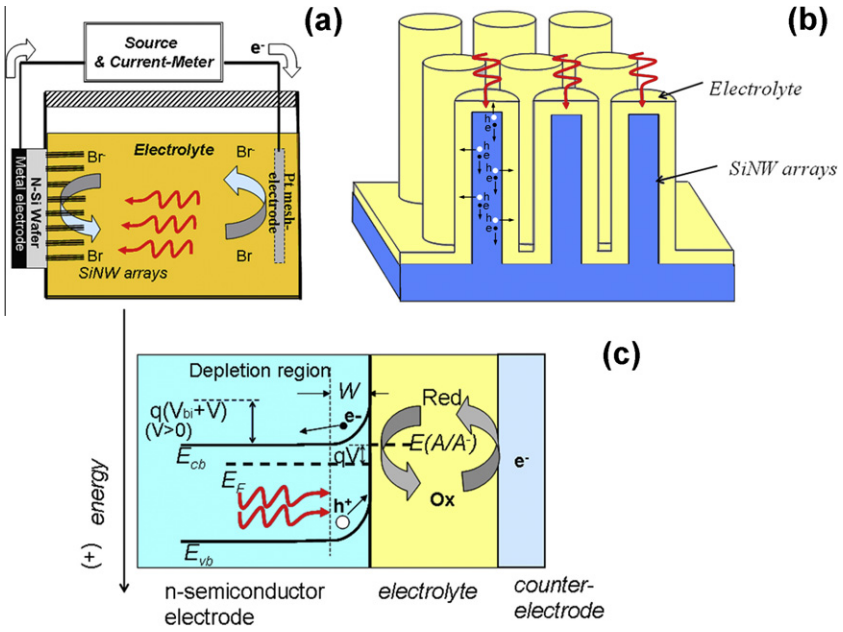

Figure 2. Schematics of photoelectrochemical response measurement configuration (a), radial 'bulk' heterostructure of the SiNW arrays/electrolyte (b), and energy band of the detector under light illumination at positive bias (c).

by band edge curvature of an n-type semiconductor under varying applied voltages [14]. When the flatband voltage (E_{fb}) is applied, there is no carrier transferred through the semiconductor/electrolyte interface, suggesting no current either in the dark or under light illumination. At an applied voltage greater than E_{fb}, there is a depletion layer, which results in that the oxidative current is limited in the dark. However, the hole density increases dramatically when the electrode is exposed to light illumination, leading to an observable photocurrent (as shown in Figure 2c). At an applied voltage smaller than $E_{fb,}$ there is an accumulation layer, which brings excess electrons at the interface. In the case, the electrode acts as a cathode both in the dark and under light illumination, causing the dark current and photocurrent to be overlapped.

It is notable that there are obvious differences in the *J–V* characteristics of the three photoelectrodes with different morphologies. As shown in Figure 4, the saturation photocurrent of the planar Si is smaller than that of the black arrays, but larger than that of the gray arrays. The applied voltages of the saturation photocurrent of the arrays are negative, but the photocurrent of the planar Si does not reach saturation until the applied voltage reaches to 0.8 V. The current density of the black arrays shows a sharper increase than that of the planar Si as the applied voltage increases. The differences in the applied voltages of saturation photocurrent and increasing rates of photocurrent come from their different morphologies. Moreover, there are slight decays of the saturation photocurrents for the array photoelectrodes, but not obvious for the planar Si. The decays are likely attributed to the oxidation of NW surfaces and an increase of inner resistance in the device, because the NWs are more easily to be oxidized due to their larger surface state density.

Different *J–V* characteristics and *R* values can be figured out by the morphology and the applied voltage, in the following four major factors. First, the SiNW arrays possess much greater surface area-to-volume ratio compared to the planar Si, as well as the excellent optical absorption. Figure 3c shows that the black arrays are almost non-reflective (the reflectance is only 1% or less) in the wavelength range of 220–1000 nm. The gray arrays show a low reflectance below 400 nm wavelength, and a slight increase of reflectance is observed when the wavelength is larger than 400 nm. However, the overall reflectance of the planar Si is over 30% in the wavelength range of 450–1000 nm. The transmission spectrum implies that the electrolyte is transparent and suitable for detecting photon whose wavelength is larger than 500 nm in this method. Second, the shapes of the semiconductor/liquid junctions for the various photoelectrodes are different. For the arrays, the shape is tri-dimensional, while for the planar Si, the shape is bi-dimensional. The tri-dimensional radial junctions usually possess a higher collection efficiency of photogenerated carriers than the bi-dimensional planar junctions [15,18]. Combining the above two considerations, one can understand that the J_{ph} and *R* of the black arrays are larger than that of the planar Si. Third, since the SiNW arrays have much larger effective surface area than the planar Si, there are more movable electrons on the NWs/electrolyte interface than on the planar Si/electrolyte interface. Consequently, the dark current density of the arrays is larger than that of the planar Si, because the three photoelectrodes were set to share the same photoactive geometric area. Finally, the bending of energy band near the surface of the NWs may be steeper than that of the planar Si when they are respectively immersed into the electrolyte of a given redox potential, which is attributed to the combination effect of Fermi-energy pining of the NWs [13] and electrochemical performances of the semiconductors [14,19]. In other words, the photogenerated carriers in the NWs may be extracted more easily than that in the planar Si. As a result, when the applied voltage is increased from 0.2 to 1.0 V, the J_{ph} of the NW arrays are nearly invariant owing to that a small bias (0.2 V) is lager enough to completely separate the photogenerated carriers; while the J_{ph} of the planar Si at 1.0 V bias shows a great enhancement compared to that at 0.2 V bias, because 0.2 V bias can not fully separate the photogenerated carrier in planar Si heterostructure, but 1.0 V bias can.

The three Si-based photoelectrodes involved in this investigation are doped in the same level, but the selection of the doping level should be careful. For an n-type semiconductor, the width (*W*) of the depletion layer within the near-surface region increases as the doping concentration reduces [20], which means that a low doping level of Si substrates brings a wide depletion layer. For the 1DSNS with a small radius (*r*), there is a reduction of recombination barrier height when the *r* is smaller than the *W*, leading to a strong

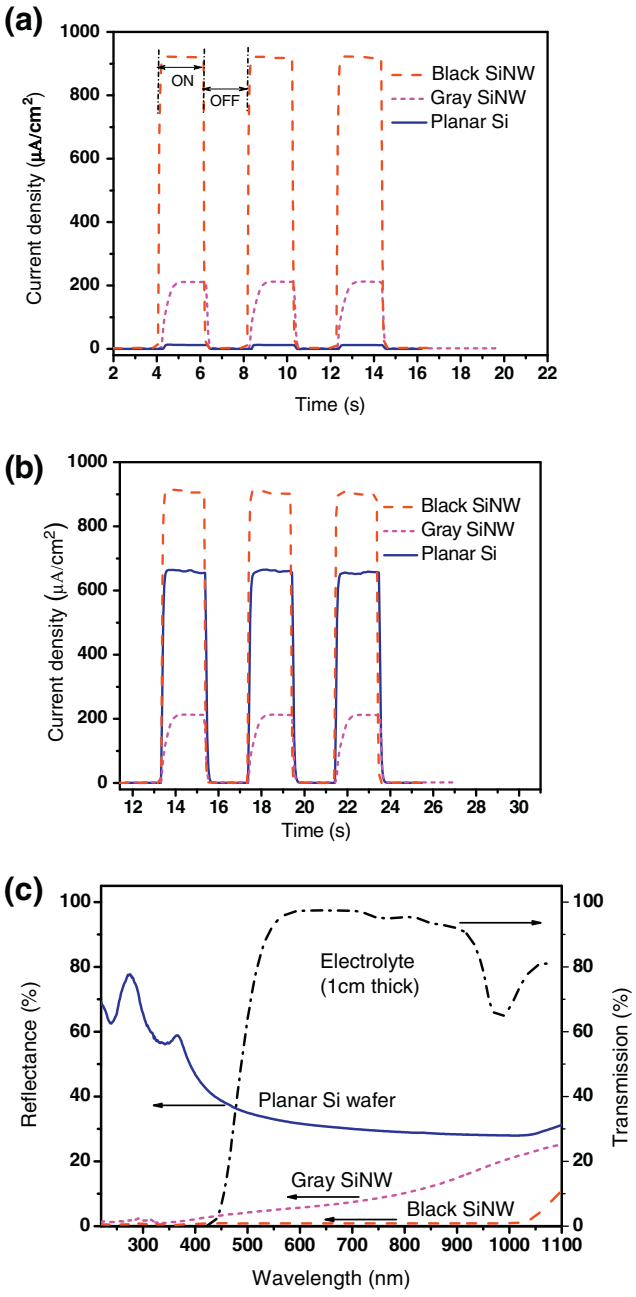

Figure 3. Current density versus time curves of the black SiNW arrays, gray SiNW arrays and planar Si under ON–OFF cycles of light illumination at 0.2 V (a) and 1.0 V (b) bias, respectively. (c) Reflectance spectra of the SiNW arrays and the planar Si, and transmission spectrum of the electrolyte.

enhancement of recombination process [13]. To ensure a high collection efficiency of photogenerated carriers, the W should be smaller than the r, so the doping concentration should be not too small. Further, increasing the doping concentration reduces the

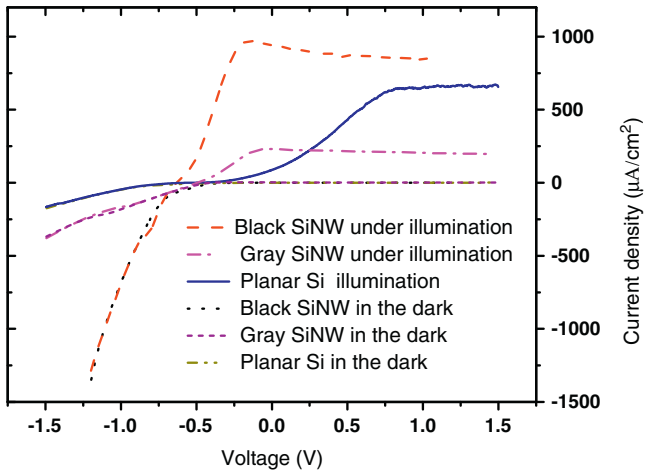

Figure 4. Current density versus potential (J–V) curves of the black SiNW arrays, gray SiNW arrays and planar Si under light illumination and in the dark, respectively.

equilibrium minority-carrier concentration at the junctions, and hence lowers the carrier recombination [21,22]. However, a too high doping level degrades the minority-carrier diffusion length L_p and brings additional deleterious processes such as the tunneling of majority carriers from the bulk through the depletion region and Auger recombination, which causes a decrease of the saturation photocurrent and an increase of the dark current [21–23]. Moreover, a high doping level usually leads to a large surface recombination at the NWs/electrolyte interface, which seriously degrades the collection efficiency of photogenerated carriers. Assuming the surface recombination is a Shockley–Read–Hall process, the rate of surface recombination (S) relates to the density of surface traps [24]:

$$S = v_t \delta N_{t,s} \gamma \tag{2}$$

where δ is the trap cross section, v_t is the carrier velocity, $N_{t,s}$ is the microscopic density of surface traps per unit projected area, and γ refers to the ratio of the true surface area to the projected surface area. Eq. (2) suggests that the S is positive correlation versus the $N_{t,s}$ and the γ. For the smooth NWs, the $N_{t,s}$ is smaller than that of the rough NWs. The γ of NW arrays is much larger than that of the planar Si ($\gamma = 1$) due to their large specific surface area. So the total S of the rough NWs is much larger than that of the planar Si, which is also experimentally demonstrated in Hagedorn's report [23]. Therefore, it can be understood that the saturation photocurrent and photoresponsivity of the gray arrays at 1.0 V bias is smaller than that of the planar Si, although the gray arrays possess better optical absorption properties than the planar Si. The roughness of the SiNWs prepared by the chemical etching method usually increases with an increasing doping concentration of Si substrates [3,25]. It indicates that the S of the SiNWs produced from heavily doped substrates is usually larger than that of the SiNWs produced from lightly doped substrates. Another two noticeable aspects-the dark current and Fermi level, are affected by the doping concentration too. Since

Table 1
Photosensitive characteristics parameters of the black SiNW arrays, gray SiNW arrays and planar Si at 0.2 and 1.0 V bias, respectively.

Parameters	0.2 V			1.0 V		
	Black SiNW	Gray SiNW	Planar Si	Black SiNW	Gray SiNW	Planar Si
J_{photo} (μA/cm²)	910 ± 8	208 ± 2.5	12.5 ± 0.5	915 ± 7	211 ± 2	664 ± 3.5
J_{dark} (μA/cm²)	2.3 ± 0.4	1.8 ± 0.1	0.1 ± 0.05	2.4 ± 0.4	2.0 ± 0.3	0.8 ± 0.2
J_{pc} (μA/cm²)	907.7	206.2	12.42	912.6	209	663.2
R(A/W)	0.583	0.133	0.008	0.586	0.135	0.426

different doping levels make the NWs showing different resistivities, and the electron density at the semiconductor/electrolyte interface is relatively high for the case of a high doping level, a relatively large dark current may be observed when the substrates are heavily doped. For an n-type semiconductor, Fermi level is usually enhanced and closer to the conduction band as the doping concentration increases around room temperatures [20]. The variation of Fermi level induces different degrees of band bending when the semiconductor is immersed into an electrolyte, which may cause the differences in the applied voltages of saturation photocurrent and increasing degrees of photocurrent with an increasing applied voltage. Consequently, the doping concentration of Si substrates should be carefully chosen, because an increase of doping concentration reduces the width of depletion layer, but increases the rate of surface recombination, and in the meantime, may improve the Fermi level and dark current during the electrochemical measurements. Therefore, the photoresponses of the SiNW arrays may be further improved by optimizing the doping concentration as well as the etching conditions.

4. Conclusions

The photoelectrochemical characteristics of the SiNW arrays prepared by a metal assisted chemical etching method were systematically investigated in the Br/Br^- electrolyte under white light illumination, with comparison to that of the planar Si. The photoresponsivity of the black arrays is 73 times larger than that of the planar Si at 0.2 V bias. These results indicate that the light detectors in the novel radial heterostructure of the 1DSNS arrays are promising. The photoresponsivity of the arrays can be further improved via the optimization of morphology, doping concentration and alternative electrolyte.

Acknowledgments

This work was supported by the National Basic Research Program of China (No. 2010CB832905), and partially by the Fundamental Research Funds for the Central Universities and the Program for New Century Excellent Talents in University (NCET).

References

[1] M.D. Kelzenberg et al., Nat. Mater. 9 (2010) 239.
[2] Y. Jiang, W.J. Zhang, J.S. Jie, X.M. Meng, X. Fan, S.T. Lee, Adv. Funct. Mater. 17 (2007) 1795.
[3] A.I. Hochbaum et al., Nature (London) 451 (2008) 163.
[4] S.W. Boettcher et al., Science 327 (2010) 185.
[5] A.P. Goodey, S.M. Eichfeld, K.K. Lew, J.M. Redwing, T.E. Mallouk, J. Am. Chem. Soc. 129 (2007) 12344.
[6] G.B. Yuan, H.Z. Zhao, X.H. Liu, Z.S. Hasanali, Y. Zou, A. Levine, D.W. Wang, Angew. Chem. Int. Ed. 121 (2009) 9680.
[7] K.Q. Peng, X. Wang, S.T. Lee, Appl. Phys. Lett. 92 (2008) 163103.
[8] A. Zhang, S. You, C. Soci, Y. Liu, D. Wang, Y.H. Lo, Appl. Phys. Lett. 93 (2008) 121110.
[9] O.L. Muskens, M.T. Borgstrom, E.P.A.M. Bakkers, J.G. Rivas, Appl. Phys. Lett. 89 (2006) 233117.
[10] H.E. Ruda, A. Shik, J. Appl. Phys. 100 (2006) 024314.
[11] M.S. Gudiksen, L.J. Lauhon, J.F. Wang, D.C. Smith, C.M. Lieber, Nature (London) 415 (2002) 617.
[12] K. Keem et al., Appl. Phys. Lett. 84 (2004) 4376.
[13] R. Calarco et al., Nano Lett. 5 (2005) 981.
[14] M.X. Tan, P.E. Laibinis, S.T. Nguyen, J.M. Kesselman, C.E. Stanton, N.S. Lewis, Principles and Applications of Semiconductor Photoelectrochemistry, John Wiley & Sons Inc., New York, 1994.
[15] L.J. Lauhon, M.S. Gudiksen, D. Wang, C.M. Lieber, Nature (London) 420 (2002) 57.
[16] M.C. Jeong, B.Y. Oh, W. Lee, J.M. Myoung, Appl. Phys. Lett. 86 (2005) 103105.
[17] Y.Q. Qu, L. Liao, Y.J. Li, H. Zhang, Y. Huang, X.F. Duan, Nano Lett. 9 (2009) 4539.
[18] B.M. Kayes, H.A. Atwater, N.S. Lewis, J. Appl. Phys. 97 (2005) 114302.
[19] A.W. Bott, Curr. Sep. 17 (1998) 87.
[20] S.M. Sze, K.K. Ng, Physics of Semiconductor Devices, third edn., John Wiley & Sons Inc., Hoboken, NJ, 2007.
[21] B.S. Simpkins, M.A. Mastro, C.R. Eddy, P.E. Pehrsson, J. Appl. Phys. 103 (2008) 104313.
[22] S.M. Wong, H.Y. Yu, J.S. Li, G. Zhang, G.Q.L. Patrick, D.L. Kwong, IEEE Electron Dev. Lett. 31 (2010) 335.
[23] K. Hagedorn, C. Forgacs, S. Collins, S. Maldonado, J. Phys. Chem. C 114 (2010) 12010.
[24] E. Yablonovitch, D.L. Allara, C.C. Chang, T. Gmitter, T.B. Bright, Phys. Rev. Lett. 57 (1986) 249.
[25] A.I. Hochbaum, D. Gargas, Y.J. Hwang, P. Yang, Nano Lett. 9 (2009) 3550.